XMaS
NEWSLETTER

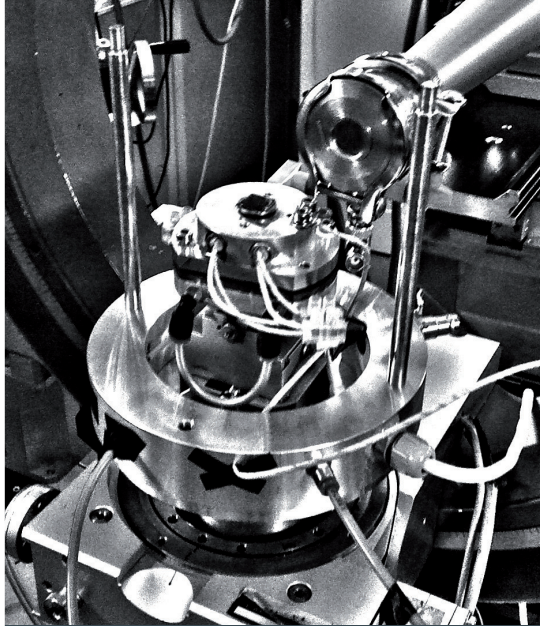

2011

Status

CONTENTS

On the cover: complex patterns in liquid crystals (main image, see article p. 15) and custom cell for controlled sample environment (top right image, see article p. 13).

It is again a very great pleasure to present the XMaS newsletter highlighting the wide range of excellent and challenging science investigated on XMaS over the last year or so together with a selection of the new developments being implemented on the beamline. The beamline continues to provide SR support to a wide range of materials science projects which underpin the RCUK Challenge Themes including Energy, Digital Economy, Healthcare Technologies as well as Research Infrastructure. Most research carried out on XMaS falls into one of the following four categories:

– **Electronic Structure** including spintronics and magnetism
– **Materials for Energy Applications** (Catalysis, Surface Science and Physical Chemistry)
– **Polymer Science**, Soft Matter and functional inorganics
– **Health Diagnostics**

Over the course of the XMaS project we have seen an increasing diversification in our portfolio. The relative number of proposals per theme has constantly evolved ever since the first Operational Phase started back in 1997. Although the beamline was originally conceived for x-ray magnetic scattering experiments, almost half of the current proposals being submitted are related to polymer science, energy and healthcare applications. Research on new materials, such as multiferroics, has strongly benefited from the cutting edge instrumentation available on the beamline. We are delighted to be able to highlight in this newsletter the strong mapping of the research undertaken on XMaS to the research themes identified by EPSRC. This illustrates the strategic need for XMaS as part of the EPSRC mid-range facility programme.

The last year has seen an expansion of our user community with several new groups coming to use the beamline. We continue to provide training opportunities to students and researchers and share best practice across the UK SR community. We also welcome an increasing number of different European users who are becoming regular users of the beamline through the ESRF access route. We anticipate that access to XMaS through this route will become even more competitive with the closure of the magnetic scattering beamline ID20, but recognise that this will only benefit the technical developments on the beamline and raise the profile of UK science to a wider European audience.

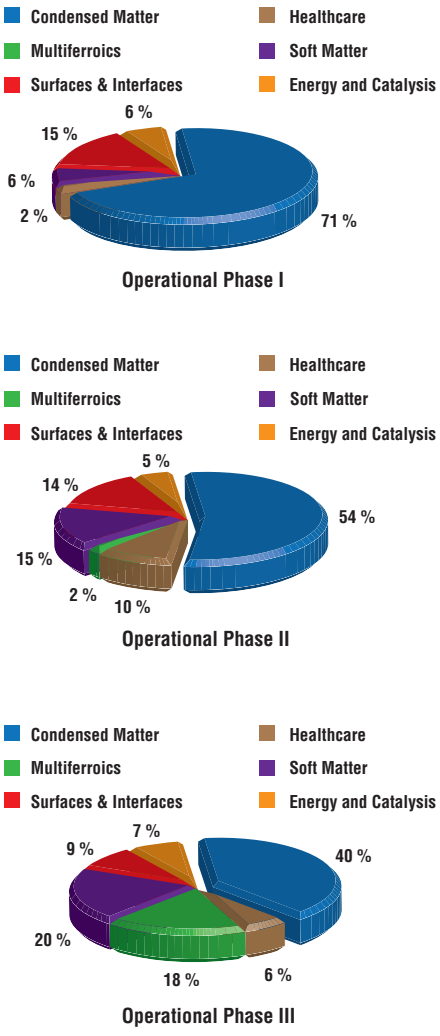

Figure 1: *EPSRC themes by proposal submission for the three operational phases of XMaS.*

The beamline staff continue to be involved with organising scientific meetings. We report on the successful meeting on multiferroics organised with the National Physical Laboratory in this newsletter. XMaS was also involved with organising the session on ''Experimental and theoretical studies of resonant X-ray scattering" at the UK Synchrotron User Meeting held at the Diamond Light Source last September. We encourage anyone with any ideas about possible meeting topics to get in touch and we will provide some support if at all possible.

With the recent creation of the Partnership for Soft Condensed Matter, XMaS users can now benefit from an extensive suite of off-line instruments and techniques that will be available before, during and after an experimental run. These facilities will be further expanded in early 2013, with a customised 800 m^2 building on the EPN site housing new laboratories with facilities to aid sample preparation and characterisation, for example, optical and electron microscopy, rheology, light scattering, etc. Projects will be aided by the availability of complex sample environments and advanced data analysis and modelling. XMaS remains a key platform for UK scientists for networking and scientific exchange. For more information please contact the local team directly.

Over the summer we have had to say goodbye to Gemma Newby as she is now completing the second part of her postdoctoral position by working on beamline I07 at Diamond Light Source. We wish her all the best for a successful future and thank her for her support and contribution to the XMaS project over the last two years. We hope that Gemma continues to work on XMaS in the future as part of our ongoing collaboration with staff and scientists at the Diamond Light Source. XMaS users coming to the ESRF site over the last year will have seen the large disruption of the road infrastructure around the EPN campus as the new tram line is installed. The ESRF itself has also turned into a building site with the onsite team being relocated around the storage ring as their office is demolished (see below) to make way for the extension of the storage ring building which forms an integral part of the ESRF upgrade. If you want to find them, they are now located on the mezzanine level close to beamline ID20.

At the time of writing the beamline is coming to the end of its third tranche of funding and we are in detailed discussions with EPSRC over continuation of funding through the mid-range facilities programme post autumn 2012. The shift from a 'responsive mode' operation to 'mid-range facility' may necessitate some changes in the way XMaS operates. This will obviously be challenging but we hope it will enable us to provide new opportunities for the UK materials community and expand what we can do and the services we offer. Fingers crossed for good news soon.

Tom Hase, Chris Lucas and Malcolm Cooper

Figure 2: *The old XMaS PLUO offices being destroyed during December 2011 to allow the extension of the experimental hall as part of the ESRF upgrade programme.*

workshops

X-ray and Neutron Scattering in Multiferroics and Ferroelectric Materials Research II

This workshop was held at the National Physical Laboratory, London on 23rd September 2011. The event brought together experts from the multiferroics, magnetoelectrics and ferroelectrics communities. Neutron and synchrotron facility users presented the latest developments in this field. A series of presentations were given by leading researchers covering a variety of topics from fundamental physics of multiferroic switching, to the latest x-ray experimental results. Other talks focused on the possibilities of using ferroelectrics as computer memory (RAM) and magnetic storage.

A discussion forum was held during the afternoon, to examine the experimental practicalities concerning the application of in-situ electric, magnetic and stress fields in x-ray and neutron experiments. Delegates also debated a wider range of issues in materials processing, crystal growth and sample preparation. The event was highly successful and brought together many leading researchers in the field enabling sharing of ideas in a pleasant, informal setting. More details about the workshop are available on the web **[1]**. The site contains a lot of practical information including a description of the different European synchrotron beamlines where in-situ studies of multiferroics are possible. A good practice guide on how to conduct ferroelectric measurements is also presented.

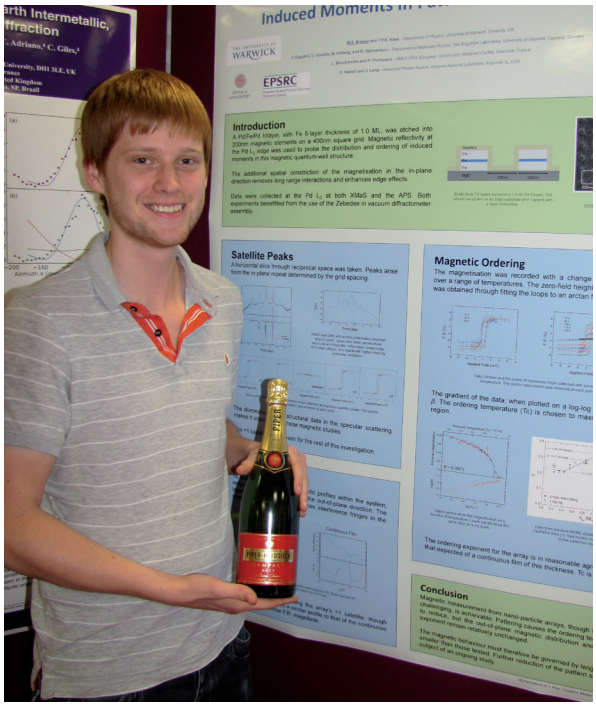

Figure 3: *Matthew Brewer from Warwick holding his prize in front of the winning poster.*

XMaS User Meeting 2011

The annual XMaS User meeting took place at the University of Warwick on 20th May 2011. Details of the technological advances made on the beamline over the last year were presented to the user community by the XMaS team. Scientific highlights from experiments performed were presented in a series of talks. The broad range of scientific work undertaken on XMaS was exemplified by the high quality presentations; Xiangbing Zeng describing his work on Liquid Crystal Honeycomb structures, Yvonne Gründer on in-situ electrochemical studies of surfaces, Markys Cain discussed electric field studies of relaxor ferroelectrics whilst Emyr MacDonald described the alignment of photovoltaic materials. Resonant magnetic scattering on the $(Rare\text{-}Earth)_2CoGa_8$ series was discussed by Roger Johnson and Mark Dowsett highlighted the possibilities of using his XEOL microscope on XMaS for cultural heritage and material studies. A summary of the revised ESRF upgrade program and how it will impact the ESRF site, XMaS users and the onsite team was also presented by Axel Kaprolat. The scientific talks were supported by a lively poster session with over 20 posters presented. The poster prize was awarded to Matthew Brewer for his resonant scattering work on FePd layers.

The user meeting continued to provide an opportunity for users to interact with the team and management. It provoked a lively discussion on the future of XMaS post 2012 and future technical developments.

[1] http://interactive.npl.co.uk/multiferroics/index.php/Multiferroics_Meeting

Low energy optimisation: update

The optimization of the beamline down to 2.4 keV is in progress. A beryllium gate-valve at the entrance of the experimental hutch is in operation and can be opened during an experiment. This valve cannot be opened unless the hutch is interlocked. A range of windowless sample environments with different 2θ angles are available for diffraction. The base temperature accessible with this fully in-vacuum setup is presently 17 K. A windowless in-vacuum polarization analyser is currently being commissioned, to further enhance the low energy capabilities of the beamline. The installation of the LN2 cooled monochromator will complete the low energy optimization of the beamline by allowing access to energies down to 2.035 keV.

6-circle geometry

The versatility of the XMaS diffractometer makes it possible to use it in different configurations. Until now, the SPEC sessions available on the beamline were restricted to 4-circle vertical or horizontal ("fourc_ver/hor"). Strictly speaking the diffractometer is a 4S+2D type. However, if the diffractometer base table tilt is used to set a low angle of incidence on a sample with its surface mounted horizontally, the diffractometer can work in 6-circle geometry. Recently, the 6-circle version of SPEC, "sixc", has been implemented and successfully tested after modifying the motor names to satisfy the 6-circle convention. This geometry is especially beneficial for surface diffraction experiments and studies of liquid surfaces or electrolytes for example.

2D pixel detectors available on loan

2D fast pixel detectors (MAXIPIX and PILATUS) from the ESRF Detector Pool, with frame rates up to 1 kHz, have been tested and used during users experiments at XMaS. The possibility of using these detectors depends on their availability, which is limited due to their high demand on other ESRF beamlines.

3D reconstruction software

A way to reconstruct stacks of 2D detector images in 3D has been completed. It makes use of the PyMca **[2]** software developed by the ESRF, which uses the EDF data format. The position of all the motors, counters, UB matrix and detector parameters are stored in the image header, making it more convenient than the MARCCD format. This information is used to get the position in reciprocal space directly from the EDF image pixels **(Figure 4**).

Automatic attenuators

The standard ESRF "autof" macro has been implemented. It automatically adjusts the attenuators so that the count-rate fits in the appropriate dynamic range of the detector used **(Figure 5**). The macro works for different types of attenuators electronics (XIA, MAATEL) and different detectors (Bicrons, Cyberstars, APD, but also 2D detectors such as Maxipix and Pilatus).

[2] http://pymca.sourceforge.net/

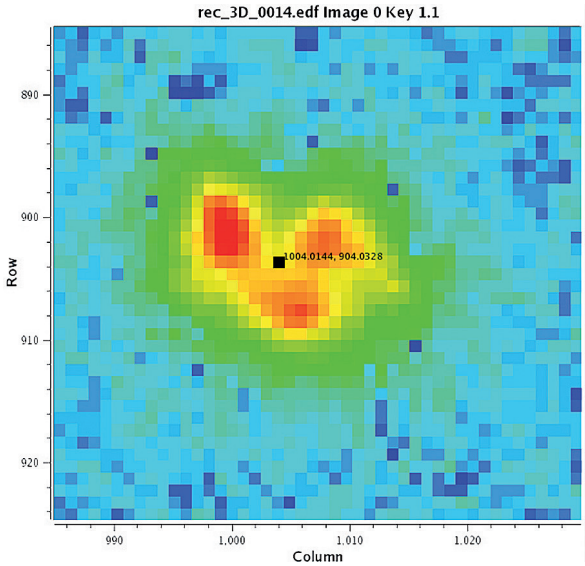

Figure 4: *MARCCD image from the (1 -1 4) Bragg peak of a holmium single crystal. The black square is at pixel (1004, 904) equivalent to (1.038, -1.060, 4.009) in reciprocal space.*

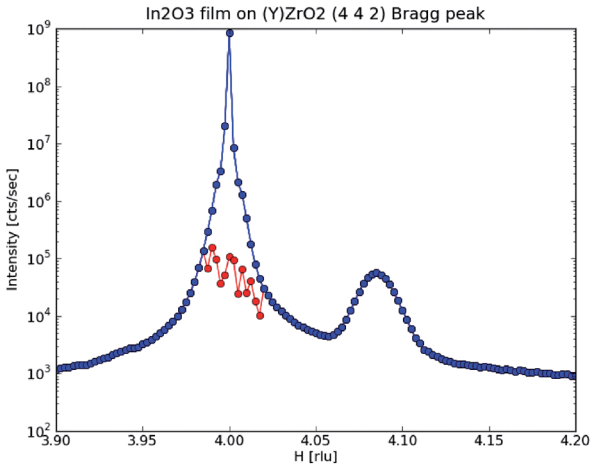

Figure 5: *In red, detector count rate measured with automatic attenuators. In blue, count rate corrected for attenuation.*

Sub 3 keV phase-plates

Diamond is generally the material of choice for x-ray phase-plates used to convert linear to circular polarised light in the 3.1 to 10 keV energy range. Above 10 keV, silicon is favoured because at these energies diamond crystals need to be thick (>1mm) and become too expensive. Yet for energies below 3.1 keV where XMaS has a unique niche it is not possible to satisfy the diffraction condition using diamond crystals and an alternative is required. Silicon remains an option but due to its very high absorption coefficient at low energies the thickness of the crystals must be chosen carefully in order to obtain circular polarization with an exploitable flux.

We report here an indirect measurement of the polarisation produced by a 5 μm thick (111) silicon phase-plate. This thin 4 mm diameter (111) silicon is supported by a 500 μm thick, 10 mm square (100) silicon frame. The polarization produced using this phase-plate was compared to a more conventional 100 μm diamond phase-plate by taking measurements at the Pd L_3 edge (3.174 keV) which covers the operational requirements of both devices.

Scattering from a ferromagnetic $[Fe(2ML)Pd(15ML)]_{x20}$ multilayer grown on a 20 nm Pd buffered (100) MgO substrate was measured at the first superlattice Bragg peak with the sample magnetization reversed at each point using an applied field of ±0.1 Tesla. The flipping ratio (FR), $(I^+-I^-)/(I^++I^-)$, where $I^\pm$ is the scattered intensity under opposite applied fields, is directly proportional to the degree of circular polarisation (P_C) incident on the sample. This ratio was measured as a function of the phase-plate angular offset (Δθ) from the Bragg angle **(Figure 6)**. The FR measured using the silicon crystal (blue curve) is maximum at Δθ=±35". For comparison, the FR measured with the 100 μm thick diamond phase-plate used in Laue transmission geometry (red curve in the inset) reaches ~±0.15% at ±180".

According to the Dynamical Theory of x-ray diffraction, a phase-shift is created between the π and σ polarisation components of an incident plane wave as it travels through a perfect crystal. Here, π and σ refer to the components of the incident electric field parallel and orthogonal to the diffraction planes of the crystal.

The angular offset where P_C is the largest is the quarter-wave plate (QWP) position where the phase-shift between the two components is exactly π/2. For the diamond, P_C corresponds to ~±90% and is only +28%, -47% for the silicon. The asymmetry of the FR measured with the silicon is attributed to the different absorption coefficients for the σ and π components as the crystal is rocked through the diffraction condition. Furthermore, the absence of any structure around the centre of the blue curve is caused by the angular divergence of the beam. This effect is more dramatic in the thin Si crystal due to the narrower angular offset required to reach the QWP position.

At 3.174 keV, the transmission of the two phase-plates is significantly different (~6% for the diamond and ~20% for the silicon) however the larger P_C produced by the diamond phase-plate clearly makes it preferable even at the expense of flux. Nonetheless, these preliminary results show that the newly manufactured 5 μm thick silicon crystals can produce circularly polarized photons at 3.174 keV and have the potential to be used as a phase-plate at low energies. The next step is to test the Si phase-plate's performance when mounted on the XMaS phase-plate flipper. This requires further technical developments of a vacuum chamber before the silicon phase-plate becomes available to users.

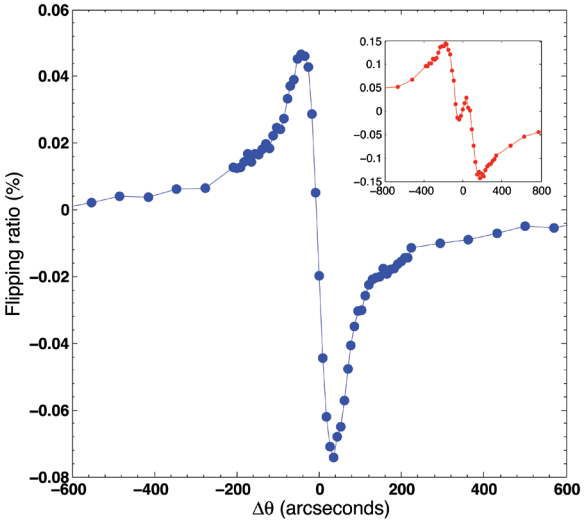

Figure 6: *Flipping ratio of $[Fe(2ML)Pd(15ML)]_{x20}$ multilayer measured at 3.174 keV as a function of the angular offset (Δθ) for the silicon (blue) and the diamond (red, inset) phase-plates. The lines are guides to the eye.*

Influence of the lattice parameter on the dielectric constant in ZrO_2 and La doped ZrO_2 thin films on Ge

A. Lamperti, C. Wiemer, A. Molle, A. Debernardi, M. Fanciulli – for more information contact: A. Lamperti, Laboratorio MDM IMM-CNR,Via C. Olivetti 2, Agrate Brianza (MB), 20864,Italy

alessio.lamperti@mdm.imm.cnr.it

The integration of high dielectric constant (κ) oxides on Ge(001) or Si(001) is a necessary step towards the scaling of future logic and memory devices. Tetragonal ZrO_2 is of particular interest due to its predicted κ value of 46.6 **[1]**. High κ values measured in thin (5-20 nm) ZrO_2 films have often been attributed to the presence of this tetragonal phase. This unambiguous signature cannot be determined with conventional x-ray diffraction, due to the difficulty in discriminating the closely spaced tetragonal and cubic reflections of ZrO_2.

Here we report on grazing incidence x-ray diffraction (GID) using wide and grazing exit angle geometry on pure and La-doped thin ZrO_2 films grown on Ge(001) by atomic layer deposition (ALD). By measuring the well isolated tetragonal (102) reflection, t(102), and by scanning the local region of reciprocal space, it was possible to simultaneously resolve the monoclinic (-121) and (112) reflections referred as m(-121) and m(112) in **Figure 7**.

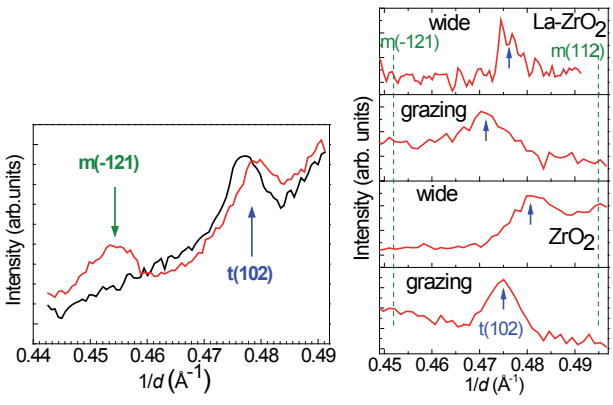

Figure 7: *GID analysis in the angular region around t(102) of La-ZrO_2 and ZrO_2 films on Ge at 9 keV: (left) 20 nm thick La-ZrO_2 before (black line) and after annealing at 400°C (red line); (right) 14 nm thick La-ZrO_2 and ZrO_2 annealed at 400°C in wide and grazing exit angle geometry. The blue arrows indicate the t(102) reflection while the green arrow indicates the m(-121) reflection. The dashed green lines show the position at which the monoclinic reflections are expected to appear.*

In the as-grown samples, the t(102) peak is detected only for thickness larger than 20 nm. After annealing, t(102) is always present and its intensity scales with film thickness. The monoclinic (-121) reflection is detected only after annealing and for films thicker than 20 nm **(Figure 7, left)**. The dielectric constant measured for as-grown La doped ZrO_2 (La-ZrO_2) on Ge(001) is 29±1, regardless of the layer thickness: after annealing, κ increases to 34±1 for the 20 and 31 nm thick films and to 42±1 for the 14 nm thick samples **[2, 3]**. By contrast, ZrO_2 grown on Si(001) gives a dielectric constant of 25±1 for the as-grown films **[4]**. The larger value of κ measured in the La-ZrO_2 films on Ge can be ascribed to a stronger polarizability of the La atoms. In annealed La-ZrO_2 films on Ge, La atoms control the Ge diffusion to an amount sufficient to further stabilize the tetragonal phase and suppress the onset of the monoclinic phase. For comparison, in La-ZrO_2 grown on Si, the same annealing promotes the monoclinic phase and subsequently the value of κ decreases.

The lattice parameters of the tetragonal structure may also severely affect the value of the dielectric constant. Variations in the peak position were found both as a function of La doping and diffraction geometry **(Figure 7, right)**, suggesting that crystals with slightly different a and c lattice parameters coexist. Given that the angle between the t(101) and t(102) directions is ~19° for the explored a and c values and that the Bragg angle of t(102) is also ~19° at 9 keV, additional Bragg-Brentano measurements of the t(101) reflection allowed us to identify lattice parameters belonging to two different families of crystals (Table I). Density functional theory calculations on un-doped ZrO_2 have demonstrated that higher κ values can be reached for values of a and c larger than the bulk, as those induced by ~2% atomic La doping **[5]**.

[1] X. Zhao, D. Vanderbilt, Phys. Rev. B 65, 075105 (2002).
[2] C. Wiemer *et al.*, ECS Transactions 35, 481 (2011).
[3] C. Wiemer *et al.*, J. Electrochem. Soc. 158, G194 (2011).
[4] A. Lamperti *et al.*, J. Electrochem. Soc. 158, G221 (2011).
[5] C. Wiemer *et al.*, Appl. Phys. Lett. 99, 232907 (2011).

	La-ZrO_2		ZrO_2	
	wide	grazing	wide	grazing
a [Å]	3.61	3.57	3.60	3.56
c/a	1.43	1.48	1.42	1.47
κ	25	25	24	24

Table I: *Measured a and c/a lattice parameters of ZrO_2 and La-ZrO_2 on Ge and calculated κ values of ZrO_2 corresponding to the lattice parameters.*

X-ray resonant magnetic scattering investigation into the bilayered iridate compound $Sr_3Ir_2O_7$

S. Boseggia, R. Springell, H.C. Walker, A.T. Boothroyd, D. Prabhakaran, D. Wermeille, L. Bouchenoire, S.P. Collins, and D.F. McMorrow – for more information contact: S. Boseggia, Diamond Light Source, Didcot, OX11 ODE, UK

stefano.boseggia@diamond.ac.uk

Recently, Ir-based transition metal oxides have attracted considerable attention. When heavy 5*d* ions are involved, effects like the crystal field and the spin-orbit interaction compete in the same energy scale giving rise to new physical properties. Among the iridates, the monolayered Sr_2IrO_4 is particularly fascinating. A recent report by Kim *et al*. **[1]** illustrated that the strong spin-orbit coupling that characterizes Ir ions, can induce a Mott instability in this compound with a localized ground state different from the conventional spin S= ½. In fact, Kim proposed a model based on a total angular momentum J_{eff} = ½ state. This model is based on the experimental observation that x-ray resonant magnetic scattering (XRMS) in a Sr_2IrO_4 crystal was strong at the L_3 edge and almost undetectable at the L_2 edge **[2].**

$Sr_3Ir_2O_7$ is the next compound along the Ruddlesden-Popper (RP) series, $Sr_{n+1}Ir_nO_{3n+1}$ from Sr_2IrO_4. It can be described as a bilayered iridate, but displays much the same bulk properties as its single layered cousin **[3]**. As one moves along the RP series the *d*-band energy width steadily increases resulting in a transition from insulating to metallic behaviour. A major question remains as to the robustness of the J_{eff} = ½ state for such changes in the electronic properties. Here we report a detailed XRMS study into the barely insulating bilayered iridate, $Sr_3Ir_2O_7$. From this investigation a series of peaks were found at (h/$_2$, h/$_2$, l) positions, which result from a commensurate ordered magnetic structure. Examples of these peaks at the (½, ½, 23) and (½, ½, 24) are shown in the inset of **Figure 9**. While all of the intensity is in the σ-π channel, the energy dependence not corrected for absorption is a Lorenzian line shape **(Figure 8)**.

By combining our XRMS data and Group Theory calculations, we have determined the magnetic structure to be a commensurate antiferromagnet consisting of two domains with propagation vectors $\mathbf{k}_1$ = (½, ½, 0) and $\mathbf{k}_2$ = (½, -½, 0). Thereby the structure factor maximises for even (odd) *l* peaks and is zero for odd (even) *l* peaks for $\mathbf{k}_1$ ($\mathbf{k}_2$) respectively.

The temperature dependence of the scattering signal shows a second order Néel transition at T_N~ 230 K for both domains. The exceptionally large ratio of Ir L_3 to L_2 edge magnetic scattering intensities observed in Sr_2IrO_4 is also present in this compound **(Figure 9)** suggesting that the J_{eff} = ½ state may still be true in this compound.

[1] B. J. Kim *et al.*, Phys. Rev. Lett. 101, 076402 (2008).
[2] B. J. Kim *et al.*, Science 323, 1329 (2009).
[3] G. Cao *et al.*, Phys. Rev. B 66, 214412 (2002).

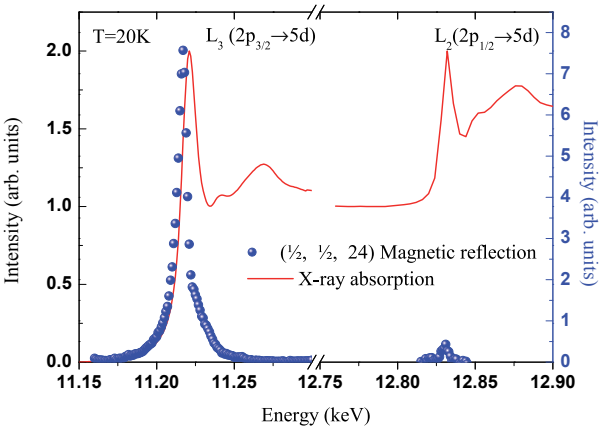

Figure 8: *Resonant enhancement of the (½, ½, 24) reflection at 20 K across the L_2 and L_3 edges in the σ-π channel. The solid red line shows the X-ray absorption normalized to the number of initial states.*

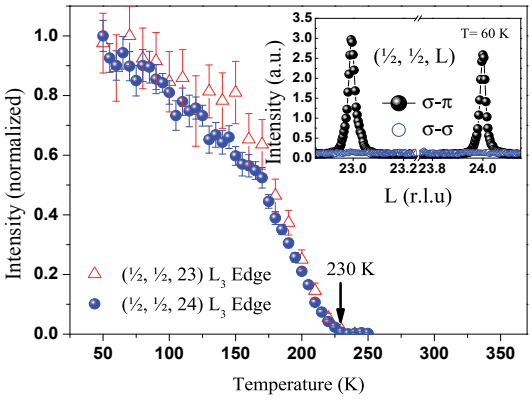

Figure 9: *Temperature dependence of the (½, ½, 23) and (½, ½, 24) peaks. Inset: L scan across the (½, ½, 23) and (½, ½, 24) at T = 60 K for the L_3 edge.*

Controlling magnetic interactions by electric field in a single phase material

P.J. Ryan, J.-W. Kim, T. Biron, P. Thompson, J.-H. Lee, X. Ke, P. Normile, E. Karapetrova, S.D. Brown, C.J. Fennie, D.G. Schlom – for more information contact: P.J. Ryan, Advanced Photon Source, Argonne, IL 60439, USA

pryan@aps.anl.gov

Direct magneto-electric (ME) coupling describes the interaction between magnetic and electric polarization through an intrinsic microscopic phenomenon in a single phase material. Systems which exhibit such coupling are potential candidates for use in a multistate logic memory storage device whereupon magnetic control with electric fields or electric control with magnetic fields could be used to alter a memory bit. We have employed x-ray resonant magnetic scattering (XRMS) to provide direct evidence of a ME cross field effect mediated through strong spin-lattice coupling in a single phase rare-earth titinate, $EuTiO_3$, film. Additionally we have established the magnetic order and the structural response to the strain imposed by the substrate.

There are multiple coexisting magnetic interactions between the 1st, 2nd and 3rd nearest neighbour (NN) Eu atoms in $EuTiO_3$ **(Figure 10, inset)**. Our DFT calculations show that the 3rd NN interaction is antiferromagnetic (AFM) and determines the G-AFM structure, the other two, on average, remain ferromagnetic (FM). The para-electric (PE) nature of this system is due to the ability to displace the Ti atom. By purposefully doing so, one can distort the alignment of the Eu-Ti-Eu bonds, and consequently reduce the strength of the magnetic interaction and thus shift the system towards a FM state.

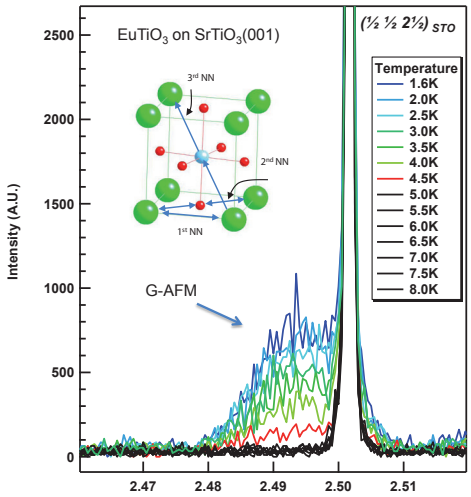

Figure 10: *Temperature dependent L scans through a half order reflection along [111] taken in σ-π geometry at the Eu L_{II} indicating the G-AFM magnetic structure of a nominally unstrained film grown on $SrTiO_3$. Inset: cartoon model showing the coexisting 1st, 2nd and 3rd nearest neighbour Eu magnetic interactions. (Red=O, Green=Eu and Blue=Ti).*

Under sufficient tensile strain the Ti is displaced permanently resulting in a ferroelectric state **[1]**. However while the system is under a nominal degree of compressive strain (LSAT(001) substrate) and remaining PE, an electric field can forcibly displace the atom distorting the Eu-Ti-Eu bond alignment **(Figure 11)**. The suppression of the 3rd NN interaction indeed leads to the emergence of the 1st and 2nd NN Eu FM interactions which begin to dominate the AFM order. This experiment clearly demonstrates cross field ME control through the coupling between polarity driven structure (Ti displacement) and the structural dependent magnetic interaction in a system with co-existing and potentially competing magnetic interactions.

It is duly apparent that in-situ XRMS with applied fields is the optimum tool to i) identify the magnetic structures of rare earth ultra-thin films (~20 nm), (ii) to measure their structural and magnetic order responses and (iii) to understand the nature underlying the coupling between structure, magnetic and electric order. This tool will exemplify itself in the study of relevant coupled phenomena like magnetoelectricity, magnetostriction and multiferoicity, to name a few.

[1] C. Chappert *et al.*, Science 280, 1919 (1998).
[2] M. Hitzfeld *et al.*, Phys. Rev. B 32, 3026 (1995).
[3] D. McGrouther *et al.*, Appl. Phys. Lett. 87, 22507 (2005).
[4] P. Warin *et al.*, J.Appl. Phys. 90, 3850 (2001).
[5] J. Desimoni *et al.*, Phys. Rev. B 48, 13266 (1993).

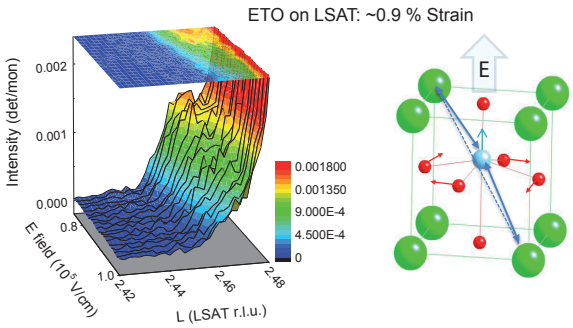

Figure 11: *L scans on a compressively strained ETO film on LSAT(001) as a function of E fields at 2K. Cartoon model illustrating how, the Ti atom displacing affects the Eu-Ti-Eu bond alignment by applying an E field.*

FIB induced intermixing in nanoscale bilayers studied by x-ray reflectivity

E. Arac, D. Burn, T.P.A Hase and D. Atkinson – for more information contact: D. Atkinson, Physics Department, Durham University, Durham, DH1 3LE UK

del.atkinson@durham.ac.uk

Highly localised control over magnetic properties such as magnetic anisotropy, coercivity and saturation magnetization in magnetic structures is desirable for applications in semiconductor and spintronic devices **[1,2]**. Lately, focused ion beam (FIB) irradiation with beam diameters ranging from 10 nm to a few μm has become a popular tool to modify and tune the magnetic properties in ferromagnetic systems. Yet there are few studies concerned with understanding the structural evolution in the material systems resulting from such FIB exposure **[3,4]**.

Our aim was to understand the structural changes occurring at the interface and the concomitant intermixing processes in nanoscale bilayer systems as a function of FIB irradiation dose. The structural changes were investigated experimentally by x-ray reflectivity and x-ray fluorescence and results were compared with theoretical models. A series of identical NiFe (20 nm)/Au (2.5 nm) bilayer structures were created by thermal evaporation through a multi aperture shadow mask onto a single Si/SiO_2 substrate. The individual structures were independently irradiated with a 30 keV focused Ga^+ ion beam with 102 nm diameter.

The specular x-ray reflectivity data for irradiated and unirradiated bilayers are presented in **Figure 12**. The solid lines are fits based upon electron density simulations. The Ga^+ dose levels are low with a Ga signal only observed in fluorescence after the highest dose. The Ga fluence does not change the effective electron density of the layers. The change in the interface structure as a function of fluence (Φ), has been followed using the interface width parameter, σ. As the irradiation dose increases, the interface between NiFe and Au becomes broader indicating significant intermixing at the NiFe/Au interface. For bilayers irradiated with fluences larger than $1.56x10^{14}$ ion/cm^2, the experimental data could not be fitted satisfactorily using a simple NiFe/Au interface. To model those structures an additional "interfacial-intermixed" layer of $Ni_xFe_yAu_{(1-x-y)}$ was added between the pure NiFe and Au layers. The thickness of this interface layer increases with increasing fluence as the diffusion depth of the intermixed atoms increases. Ion-induced intermixing at the interface can be studied by the fluence dependence of the squared total intermixing length, $X^2(\Phi)$ **[5]**, where X is defined as the total interface width (σ) between the NiFe and Au layers plus the thickness of any interfacial-intermixed layer. **Figure 13** shows the X^2 as a function of irradiation fluence. The linear dependence implies that FIB induced mixing operates in the diffusion-controlled regime. The slope of fit provides the mixing rate, $k=X^2/\Phi$, which can be used to determine the mixing mechanism which was found to be 1.7 nm^4. Theoretical mixing rates using ballistic and thermal models are 0.27 nm^4 and 1.8 nm^4, respectively. Our data show that focused Ga^+ ion irradiation induces thermally controlled mixing.

[1] C. Chappert *et al.*, Science 280, 1919 (1998).
[2] M. Hitzfeld *et al.*, Phys. Rev. B 32, 3026 (1995).

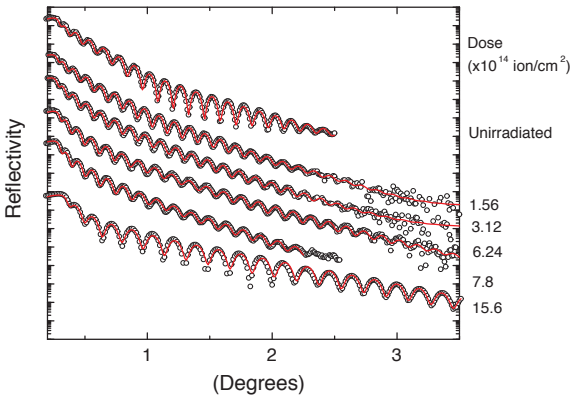

Figure 12: *Experimental x-ray reflectivity data points (circles) and corresponding best fit curves for NiFe/Au structures irradiated with different Ga fluences. Curves with increasing fluence have been shifted for clarity.*

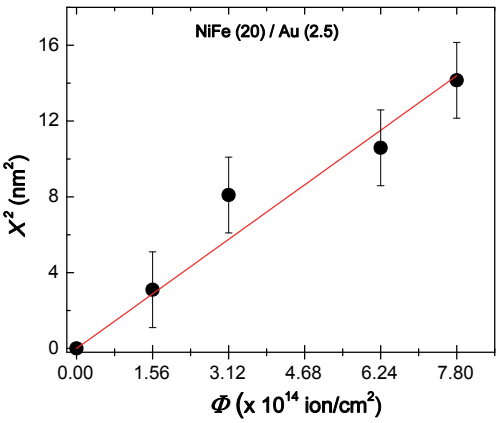

Figure 13: *Squared intermixing length as a function of irradiation fluence, Φ. The solid line is a fit to the data points.*

Probing strain in In_2O_3 thin films

K.H.L. Zhang, A. Regoutz, R.G. Egdell, A. Walsh, D. Wermeille and R.A. Cowley – for more information contact R.G. Egdell, Department of Chemistry, Inorganic Chemistry Laboratory, South Parks Road, Oxford OX1 3QR, UK.

russell.egdell@chem.ox.ac.uk

Transparent conducting oxides (TCOs) combine the properties of optical transparency in the visible region with a high electrical conductivity, and have widespread application as window electrodes in photovoltaic devices, liquid crystal displays and organic light emitting diodes. In_2O_3 is a prototypical TCO, which is amenable to degenerate n-type doping with Sn to give so-called indium tin oxide (ITO). In spite of the undoubted technological importance of ITO, many of the basic physical properties of In_2O_3 itself have proved to be controversial, including the nature and magnitude of the band gap. This is a critical parameter for a TCO. Based in part on hard X-ray photoemission measurements conducted on beamline ID16 at the ESRF, it was established in 2008 that In_2O_3 has a direct but dipole forbidden bandgap of 2.9 eV, which is almost 1 eV lower than the widely quoted gap of 3.75 eV that marks the onset of strong optical absorption **[1]**.

More recently it has been shown that the allowed and forbidden bandgaps can both be modified by epitaxial strain when In_2O_3 is grown on cubic Y-stabilised ZrO_2 whose lattice spacings are around 1.6% bigger than those of In_2O_3. This opens the possibility of using strain to tune the bandgap for device applications. First principles density functional theory calculations **[2]** reveal that the magnitude of the reduction of the bandgap depends critically on the exact numerical value of the Poisson ratio – the parameter that links longitudinal compression with transverse expansion. Until recently however there has been no reliable experimental value for the Poisson ratio. The missing piece in this jigsaw was provided by experiments conducted on the XMaS beamline this year in which in-plane expansion and out-of-plane contraction were measured by reciprocal space mapping of non-specular reflections from high quality samples **(see Figure 14)** grown by plasma assisted molecular beam epitaxy (MBE) **[3]**. Typical results are shown in **Figure 15** allowing us to derive a value of 0.31 for the Poisson ratio. This work provides a sound basis for using strain to engineer the bandgap in ITO thin films and heterostructures.

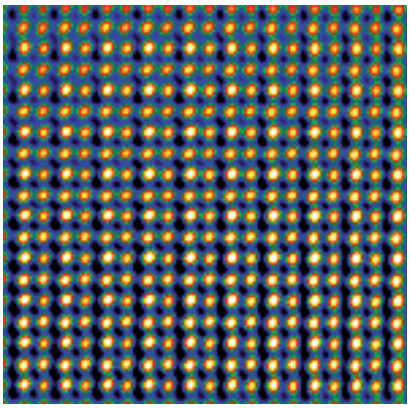

Figure 14: *High resolution TEM image of In_2O_3 epilayer grown on (001) oriented cubic zirconia by O-plasma MBE and viewed down the [100] direction. High quality films of this sort were used in reciprocal space mapping experiments.*

[1] A. Walsh *et al.*, Phys. Rev. Lett. 100, 167402 (2008).
[2] A. Walsh *et al.*, Phys. Rev. B 83, 161202 (2011).
[3] K.H.L. Zhang *et al.*, Phys. Rev. B 84, 233301 (2011).

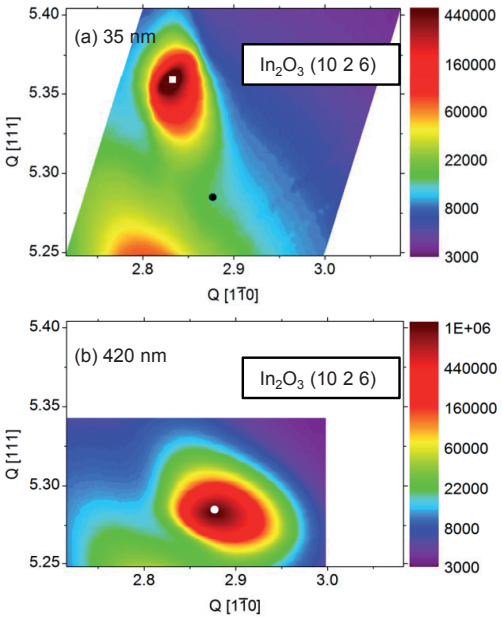

Figure 15: *Reciprocal space maps of the (10 2 6) reflection from two In_2O_3(111) thin films of different thicknesses grown on cubic zirconia (111) by MBE. The circular spots - black in (a), white in (b) - mark the positions in the map for bulk unstrained In_2O_3. The thinner film is highly strained with the maximum in the scattering intensity - indicated by a white square - strongly displaced from unstrained In_2O_3 whereas the thicker film is almost completely relaxed so that the scattering intensity peaks close to the value for bulk In_2O_3.*

Distribution of enamel crystallite orientation through an entire tooth crown studied using synchrotron x-ray diffraction

L.M. Simmons, M. Al-Jawad, S.H. Kilcoyne, D.J. Wood – for more information contact: M. Al-Jawad Institute of Dentistry, Queen Mary University of London, Mile End Road, E1 4NS, UK

m.al-jawad@qmul.ac.uk

Dental enamel is the hardest and most mineralised substance in the human body, with 96% mineral content by weight in the form of a non-stoichiometric calcium hydroxyapatite (HA), $Ca_{10}(PO_4)_6(OH)_2$. As a result of the biomineralisation process during enamel formation, it adopts a highly oriented, hierarchical structure. The structural organisation within enamel linked to its mechanical properties ensures it meets its functional requirement as a biomineral for cutting, grinding, and mastication. In our previous investigations we have shown how synchrotron x-ray diffraction (XRD) studies on the XMaS beamline can be used to probe the spatial variations in lattice parameter and texture distribution of HA crystallites across the enamel of intact healthy tooth sections **[1]**. Now, we have used position-sensitive XRD on XMaS to quantify the spatial variation in the direction and magnitude of the preferred orientation of enamel crystallites across a whole tooth crown in three dimensions by cutting the tooth into several sections.

MARCCD images were collected with a 300 μm x 300 μm beam spot and every 300 μm over a series of six sequential tooth sections obtained from a single maxillary first premolar. Following Rietveld refinement of all diffraction patterns, the texture coefficient values were constructed into 2D texture-distribution contour maps. Individual contour maps showing the change in magnitude of preferred orientation for each of the tooth sections are shown in **Figure 16**. It can be seen that there is less texture in the surface enamel at both the buccal and palatal sides of the tooth **(Figure 16a and f)** than in the central mesio–distal slices. In addition, **Figure 16b**, **c** and **e** indicate a higher degree of preferred orientation at the cusp. In contrast, the most central slice **(Figure 16d)** highlights a decrease in the texture along the top of the tooth slice. Both the magnitude and direction of the crystallite orientation was found to have a high spatial heterogeneity. Areas of high crystallite alignment were directed perpendicular to the biting surfaces which is thought to meet the functional requirements of mastication.

The results suggest that cavity preparation design may benefit by taking into account the degree of enamel crystallite orientation in the surrounding sound enamel in order to maximise fracture resistance following a restorative procedure **[2]**. Further intratooth investigations into the variation in crystallographic properties of enamel will allow a deeper understanding of the structure–function relationship and the evolutionary development of the complex hierarchical ultrastructure of enamel.

[1] M. Al-Jawad *et al.*, Biomaterials 28, 2908-2914 (2007).
[2] L.M. Simmons *et al.*, Eur. J. Oral Sci. 119, 1–6 (2011).

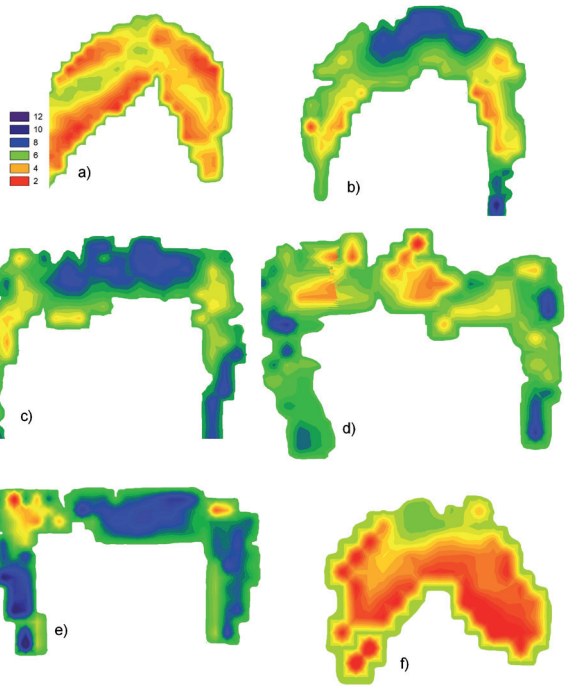

Figure 16: *Magnitude of preferred orientation of the (002) reflection of hydroxyapatite crystals in enamel for six intact tooth sections cut along the mesial–distal plane: (a) buccal section, (b–e) central section, (f) palatal section.*

Surface structures of pluronics

G. Newby, B. O'Driscoll and O. Bikondoa – for more information contact G. Newby, Diamond Light Source Ltd, Didcot, OX11 0DE, UK

gemma.newby@diamond.ac.uk

Pluronics are a group of non-ionic amphiphilic, tri-block copolymers used in a variety of applications from drug delivery **[1]** to microfluidics **[2]**. Pluronics® is the trade name used by BASF; they are also known as Poloxamers and Synperonics.

Pluronics exhibit very rich phase behaviour **[3]** enabling them to be exploited in many sectors. In this study the surface properties of Pluronic P85, $PEO_{26}PPO_{41}PEO_{26}$ **(Figure 17)**, have been probed in order to enhance the prospective industrial applications of these remarkable materials. Large arrays of cubic and hexagonal structures are in high demand especially in the biotechnological sector. Pluronics can achieve these desired structures under controlled environments.

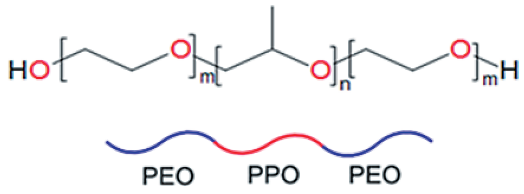

Figure 17: *Structure of Pluronics®: polyethylene oxide / polypropylene oxide / polyethylene oxide with their respective acronyms PEO/PPO/PEO.*

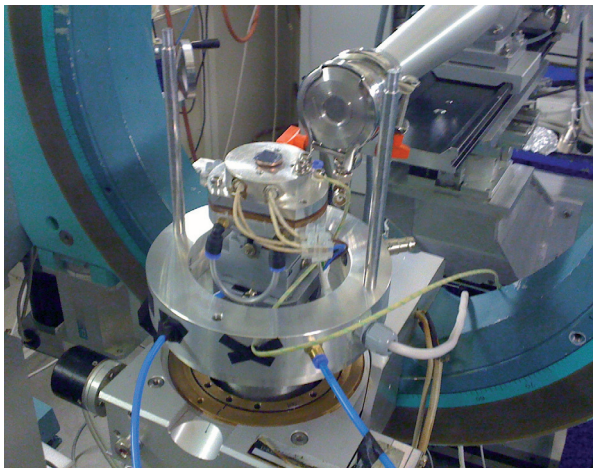

Figure 18: *Setup showing the temperature and humidity cell without the kapton cover.*

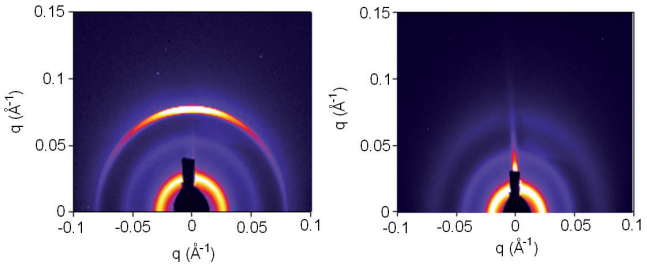

Figure 19: *GISAXS patterns of a 35 wt% P85 on a hydrophobic silicon wafer measured at 9 keV at two different temperatures. The left image taken at 30 ºC can be indexed to a hexagonal close packed array. The structure shows quasi–isotropic behaviour. The right hand image was taken at 45°C and shows a lack of hexagonal order and a melting into a correlated micellar phase.*

The degree of ordering of P85 was evaluated by means of grazing incidence small angle x-ray scattering (GISAXS) in a controlled sample environment. The temperature was regulated with a Peltier-cooled plate. The humidity was kept constant by bubbling helium through a water line **(Figure 18)**.

We observed that P85 is subject to remarkable changes in morphology with both temperature and humidity. When any of the concentrations dry out, an expected lamellar phase forms as a result of the hydrophobic effect. On the other hand, if humidity is maintained, the surface structure is modified depending on concentration and temperature. For example, **Figure 19** shows GISAXS patterns of a specific concentration of P85 deposited on a hydrophobic surface. Structural changes were observed with increasing temperature whilst in a constant humidity environment.

In conclusion a variety of structures are present in these systems from correlated micelles to mesoporous arrays confirming the high tunability of Pluronics. The surface morphology of selected concentrations of Pluronic P85 has been understood. Our wider aim is to generate a morphology diagram that will allow conditions to be chosen for the required application. For example protein folding requires a cubic to hexagonal transition at ambient temperatures. The structural order produced by these systems could be technologically extremely important especially if it can be stabilised over a large area. A large domain size is also desirable for many applications such as in biosensors.

[1] K. Huang *et al.*, Polym. Preprints 42, 147 (2001).
[2] V.N. Luk *et al.*, Langmuir 24, 6382 (2008).
[3] G.E. Newby *et al.*, J. Colloid Interf. Sci. 329, 54 (2009).

Structured nanofilms via ionic self-assembly

T.G. Dane, P.T. Cresswell, O. Bikondoa, G.E. Newby, T. Arnold, C.F.J. Faul, W.H. Briscoe – for more information contact: W.H.Briscoe, School of Chemistry, University of Bristol, UK

wuge.briscoe@bris.ac.uk

Conducting organic polymers offer promising application in flexible electronic and optoelectronic devices. One of the main challenges when working with such materials is to achieve a well-organised supramolecular structure of the constituent components, particularly when confined in nanoscale films. This is due to structural defects such as chain-coiling and entanglement inherent to the polymeric nature of the materials, which inhibit the charge mobility through the polymer and reduce the observed conductivity.

We have recently demonstrated **[1]** the feasibility of achieving well-defined lamellar structure in conducting nanofilms taking a two-pronged approach: 1) we used short oligomeric analogues (tetramers and octamers) of poly(aniline) (PANI, a widely studied conducting polymer) to overcome the inherent disorder and poor solubility associated with polymers, and 2) to these oligomers we added BEHP, a phosphate diester surfactant (chemical structures shown in **Figure 20**), to activate the conductive property and to induce self-assembly through the ionic interaction of chemical building blocks.

Oligomer films of thickness 40 and 400 nm were prepared by drop casting and solvent annealing onto a silicon substrate. Synchrotron X-ray reflectivity (XRR) was used to examine the organisation of the nanofilms. **Figure 21** shows an example XRR curve for a 400 nm film of the aniline tetramer doped with BEHP. The presence of the sharp Bragg peaks indicates unequivocally the formation of lamellae lying parallel to substrate.

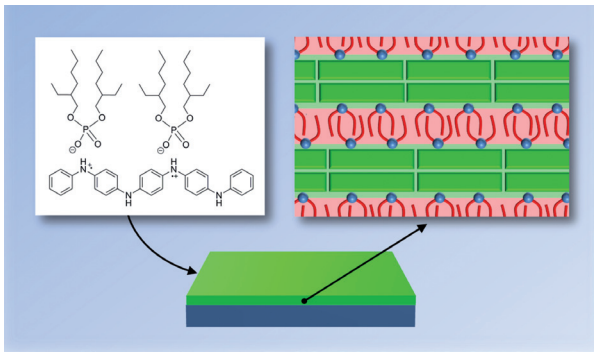

Figure 20: *Chemical structures and resulting lamellar organisation for the aniline tetramer (shown as green layers) and surfactant BEHP (shown as red layers).*

In general, we found that the lattice spacing of the multilayered structure depends on the oligomer chain length, the ratio of oligomer to surfactant and film thickness. For films of thickness 40 nm we did not observe the formation of the lamellar structure present in thicker films. The formation of well-defined lamellar structure in our oligomer nanofilms may be attributed to a number of intermolecular interactions.

These interactions include the Coulomb forces between the acid surfactant and the oligomer, the π-π interactions between neighbouring oligomers and the van der Waals forces between the surfactant tails, which all promote structure formation. However at the air-film interface, the rapid evaporation of solvent could lead to disorder in surface layers of some tens of nanometers which inhibits the self-assembly process. For the 40 nm thick samples this disorder disrupts structure formation, however when the film is thicker, around 400 nm in our case, self-organisation prevails in the film.

We may derive further information on the nature of organisation within the film by examining the shape of the Bragg diffraction peaks **[2]**. For certain samples a large ordered domain was found to exist within the film, with the domain size up to 100 nm, although this parameter depends on the oligomer and quantity of surfactant present.

We have thus demonstrated a facile route to produce highly ordered nanoscale films of conducting organic materials.

[1] T.G. Dane *et al.*, Soft Matter (2011) in press, DOI:10.1039/C2SM06492H.

[2] S. Lilliu *et al.*, Macromolecules, 44, 2725 (2011).

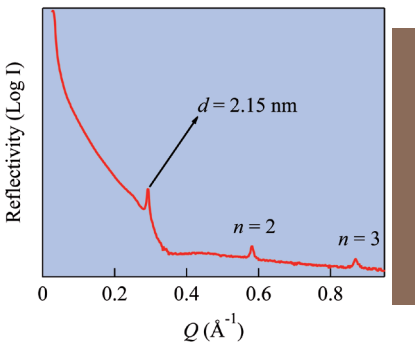

Figure 21: *XRR curve for a 400 nm film of oligo(aniline)-surfactant complex. Diffraction peaks arising from a lamellar structure are observed.*

Multicolour liquid crystal honeycombs

X.B. Zeng, F. Liu, G. Ungar, B. Glettner, T. Tschierske – for more information contact: G. Ungar, Department of Materials Science and Engineering, University of Sheffield, Sheffield S1 3JD, UK

g.ungar@sheffield.ac.uk

Through molecular self-assembly liquid crystals (LC) can form complex nanoscale patterns, which can be used as functional materials. Here we study molecules consisting of a rigid rod core capped at each end with hydrogen-bonding groups and having one or two flexible non-polar side chains - see e.g. **Figure 22**. These compounds have been found to assemble in honeycombs (HC) with cells of different polygonal cross-sections **[1]**. The rods form the cell walls ("wax"), while the side-chains ("honey") fill the cells. The larger the side-chain, the more sides to the polygon. Thus compounds with small chains form triangular cells, while those with longer chains can form anything from squares to extended hexagons. If, as in Compound 1, the two side chains are incompatible, they will tend to occupy separate cells. Triangular, square or trihexagonal (kagome) HCs were recently obtained with cells of two different chemical compositions, or "colours" **[2]**.

However, by introducing frustration into the system, one can obtain highly complex structures. Thus if the side-chains are long enough to form a hexagonal HC, clean phase separation between the two chain types is impossible - the frustration is similar to that of an antiferromagnet on a triangular lattice; all three spins on a triangle cannot be antiparallel. Thus a "two-colour" hexagonal HC is observed in the LC, with one pure for every two mixed cells **[3]**. A second order transition to a "paramagnetic" phase with all cells mixed occurs on heating such a structure.

More elaborate "multicolour tiling" patterns are achieved if, for example the chains are too large for triangular cells and remain too small to form square cells. Aligned thin films of X-shaped LCs were studied using grazing incidence small-angle x-ray scattering (GISAXS). **Figures 23a** and **b** show GISAXS patterns

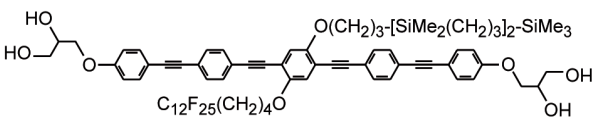

Figure 22: *Example of X-shaped polyphiles: Compound 1.*

of two HC phases of Compound 1. Superimposed on the GISAXS patterns are the corresponding 2D reciprocal lattices in several orientations. Although the molecules are small (ca 3 nm), the unit cells are large: 21 x 11 nm for the high-temperature phase. Electron density maps were constructed **(Figures 23c and f)**. To explain the maps, schematic molecules are superposed, bearing in mind that the perfluoro-chains have the highest (blue-purple) and the carbosilane the lowest electron density (red). It emerges that the low-temperature phase is a HC composed of pure carbosilane triangles **(red, Figure 23e)**, pure fluoroalkyl rhombuses (dark blue) and squares in which the two chains are mixed (light blue).

The high-temperature phase is even more complex. This honeycomb contains 18 channels in a unit cell. They are of five different colours (compositions) and four different shapes, shown in **Figure 23h [3]**. The red ellipses drawn on the maps suggest that the phase may be one step away from a quasicrystal with twelve-fold symmetry, a kind of structure that earned Daniel Shechtman this year's Nobel prize for Chemistry.

[1] G. Ungar *et al.*, Adv. Funct. Mater. 21, 1296 (2011).
[2] B. Glettner *et al.*, Angew. Chem. Int. Ed. 47, 9063 (2008).
[3] X.B. Zeng *et al.*, Science 331, 1302 (2011).

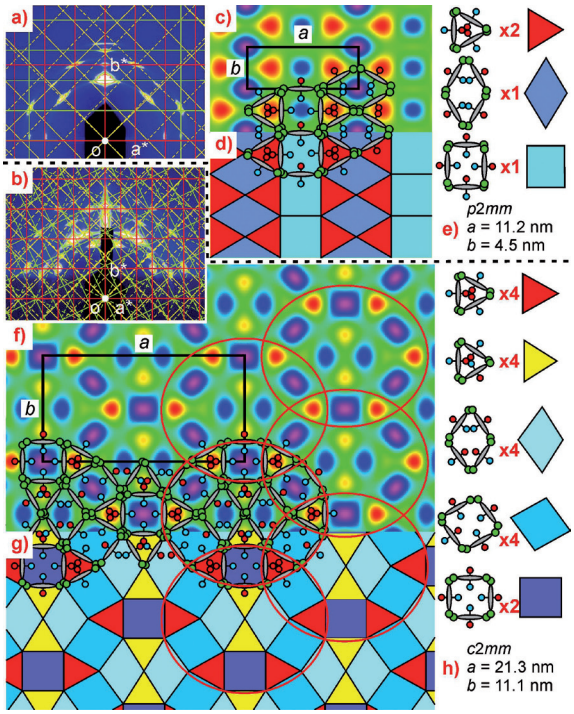

Figure 23: *(a,b) GISAXS patterns, (c,f) electron density maps and (d,g) schematic tiling representations of the low- and high-temperature phases of Compound 1. (h) The five tile types in the high-temperature HC.*

Optimising molecular organisation in organic photovoltaic blends

S. Lilliu, T. Agostinelli, M. Hampton, E. Pires, J. Nelson and J. E. Macdonald, School of Physics and Astronomy, Cardiff University, Department of Physics, Imperial College, London UK

macdonald@cf.ac.uk

Photovoltaic (PV) panels based on crystalline semiconductors such as silicon are relatively expensive to produce and process for large-area applications. Organic photovoltaic materials offer cheap, large area processing on flexible substrates, particularly attractive for diffuse lighting and for versatility. Organic PV efficiencies have increased dramatically over the last decade, promising large-scale, wider applications **[1]**. Most organic PV devices are based on thin films comprising an electron accepting component (such as a fullerene derivative) and an electron donating component (usually a conjugated polymer) between two electronically different electrodes **(Figure 24)**. The limiting factor for efficiency is the short exciton diffusion length of ~10 nm requiring photogeneration close to an interface in a bi-continuous network of donor and acceptor paths.

We have investigated two strategies for improving the molecular ordering in polymer photovoltaic blends. In PCPDTBT:PCBM blends **(Figure 25)** we have explored the use of octanedithiol (ODT) additive. In **Figure 26**, it is seen that PCPDTBT processed with ODT, shows considerably sharper (100) and (010) peaks and their positions change slightly. Likewise the blend processed with ODT shows a strengthening of the (100) peak arising from the inter-chain stacking **[2]**.

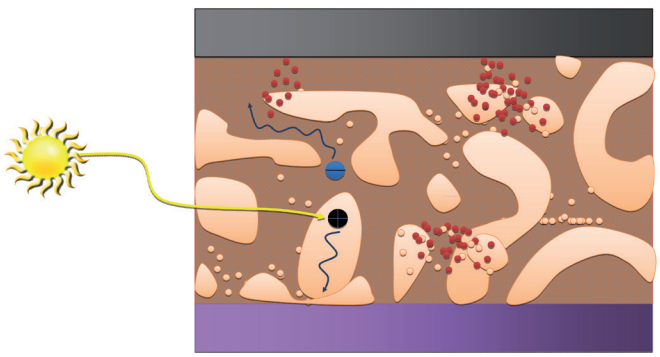

Figure 24: *A continuous flow of donors (pale brown) and acceptors (dark brown) guarantees a charge transfer between the two electrodes (grey and magenta bands).*

We have also probed the effect of annealing on blends of regioregular poly(3-hexylthiophene) (P3HT) blends with PCBM for different compositions in real time **(Figure 27)**. The domain size increases dramatically during the first two minutes of annealing, consistent with the observed increase in photovoltaic efficiency.

[1] G. Dennler *et al.*, Adv. Mater., 21, 1323 (2009).
[2] T. Agostinelli *et al.*, J. Polym. Sci. Pol. Phys. 49, 717 (2011).
[3] T. Agostinelli *et al.*, Adv. Func. Mater., 21, 1701 (2011).

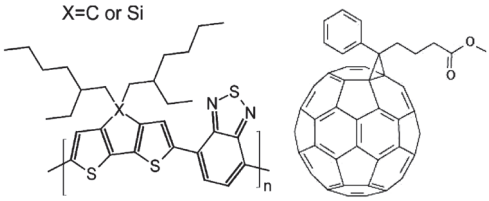

Figure 25: *Molecular structure of poly[2,6-(4,4-bis-(2-ethylhexyl)-4H-cyclopenta[2,1-b;3,4-b']dithiophene)-alt4,7(2,1,3-benzothiadiazole)] (PCPDTBT) and[6,6]-phenyl butyric acid methyl ester (PCBM).*

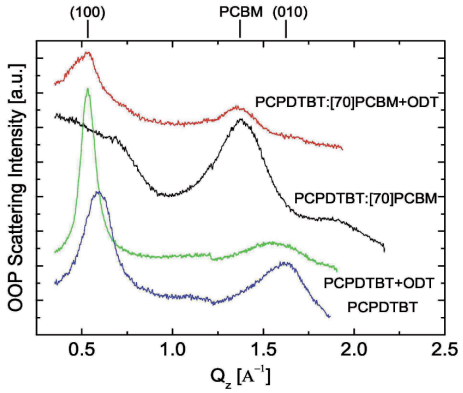

Figure 26: *Out-of-plane (OOP) diffraction profiles for PCPDTBT and PCPDTBT:[70]PCBM films processed with and without ODT [2].*

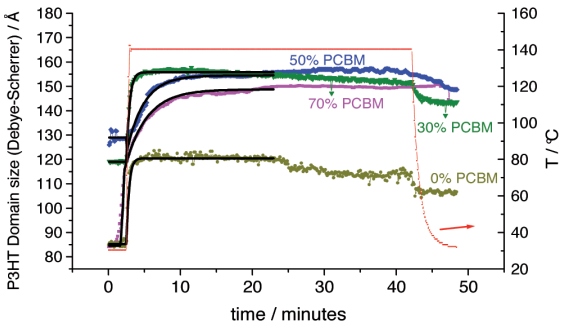

Figure 27: *Domain size of P3HT:PCBM blends in real time during annealing at 140°C after correction for paracrystallinity [3]. The sample temperature is shown in red.*

The atomic structure of the electrochemical double layer

C.A. Lucas, P. Thompson, Y. Gründer and N.M. Markovic – For further information contact C.A. Lucas, Department of Physics, University of Liverpool, Liverpool, L69 7ZE, UK

clucas@liverpool.ac.uk

The design and synthesis of energy efficient and stable electrochemical interfaces (materials and double layer components) for accelerating and directing chemical transformations is the key to developing new alternative energy systems. In aqueous electrolytes, depending on the nature of the reacting species, the supporting electrolyte and the metal electrodes, two types of interactions have traditionally been considered: (i) direct – covalent bond formation between adsorbates and electrodes, involving chemisorption, electron transfer and release of the ion hydration shell; and (ii) relatively weak non-covalent metal-ion forces that may affect the concentration of ions in the vicinity of the electrode but do not involve direct metal-adsorbate bonding. Although these findings have established the importance of non-covalent interactions in surface chemistry, many questions from the previous studies have remained open; a central issue being the determination of the position of hydrated cation clusters in the compact part of the double layer.

Here we present the structure of the electrochemical double layer at the interface between a Ag(111) electrode and 0.1 M KOH electrolyte probed using in-situ surface x-ray diffraction **[1].** In order to derive a structural model for the interface, crystal truncation rod (CTR) data were measured at fixed potentials (-1.0 V and -0.2 V) **(Figure 28)**. A schematic illustration of the interface structures determined from the CTR measurements is shown in **Figure 29** and summarises the results. At E= -1.0 V, where there is no chemisorbed species on the surface, the CTR measurements are consistent with the presence of an hydrated cation adlayer at a distance of 4.1 Å above the Ag surface. At E= -0.2 V, however, OH_{ad} stabilises the hydrated K^+ cations, at a distance of 3.6 Å above the Ag surface, through a non-covalent (van der Waals) interaction.

Although the results presented here are specific to the Ag(111) electrode in alkaline solution, both the methodology and results are important in developing an understanding of the role that the compact electrolyte layer at the interface (and the specific cation in solution) plays in determining the kinetics of electrochemical reactions that occur in this potential range.

[1] C. A. Lucas *et al.*, Electrochem. Comm. 13, 205 (2011).

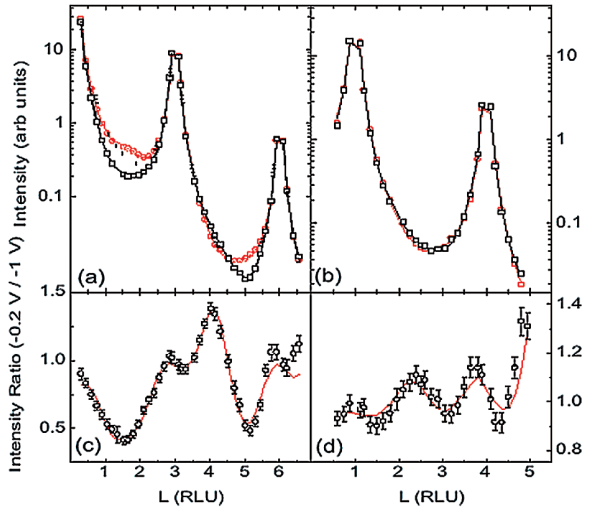

Figure 28: *CTR data of the Ag(111)/0.1M KOH interface measured at -1.0 V (circles) and -0.2 V (squares): (a) the specular CTR (0, 0, L) and (b) the non-specular CTR (1, 0, L). The CTR data measured at -0.2 V are normalized to the data measured at -1.0 V in (c) and (d). The solid lines are fits to the data and the dashed line in (a) is a calculation without inclusion of any ordering in the electrolyte.*

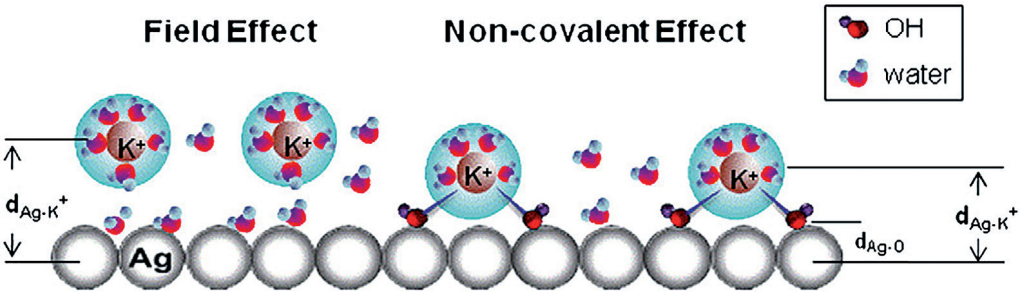

Figure 29: *Schematic illustration of the interface structure at the negatively charged (left) and positively charged (right) surface. The layer separations obtained from the CTR measurements are indicated.*

➡ Please note

Some of the experimental reports in the previous pages are as yet unpublished. Please email the contact person if you are interested in any of them or wish to quote these results elsewhere.

➡ Our web site

This is at:
www.esrf.eu/UsersAndScience/Experiments/CRG/BM28/
It contains the definitive information about the beamline and the on-line beamline manual.

➡ Living allowances

These are still 55 euros per day per beamline user—the equivalent actually reimbursed in pounds sterling, of course. XMaS will support up to 3 users per experiment. This is not a restriction on the number of experimentalists but you should make your own budgetary arrangements for those in excess of 3. The ESRF hostel still appears adequate to accommodate all our users, though CRG users will always have a lower priority than the ESRF's own users. Do remember to complete the web-based "A form" requested of you when you receive the ESRF invitation. All attendees must be listed, since this informs the safety group of the attendees and is used to organise all site passes, meal cards and accommodation.

➡ Beamline people

The personnel changes which occurred during the last fifteen months were described in the Introduction to this Newsletter.
Beamline Responsible – Simon Brown (sbrown@esrf.fr).
Beamline Coordinator – Laurence Bouchenoire, (boucheno@esrf.fr), is the person who can provide you with general information about the beamline, application procedures, scheduling, etc. Laurence should normally be your first point of contact.
Beamline Scientists – Simon Brown (sbrown@esrf.fr), Oier Bikondoa (oier.bikondoa@esrf.fr) and Didier Wermeille (didier.wermeille@esrf.fr).
Technical Support – Paul Thompson (pthompso@esrf.fr) continues to work on instrument development and provides technical support for the beamline. John Kervin (jkervin@liv.ac.uk), who is based at Liverpool University, provides further technical back-up and spends part of his time on-site at XMaS.
Project Directors – Malcolm Cooper (m.j.cooper@warwick.ac.uk), Chris Lucas (clucas@liv.ac.uk) and more recently Tom Hase (T.P.A.Hase@warwick.ac.uk) continue to travel between the UK and France to oversee the operation of the beamline. The administration for XMaS continues to be handled by Sandra Beaufoy at Warwick University (s.beaufoy@warwick.ac.uk).

➡ The Project Management Committee

The current membership of the committee is as follows:
- Bob Cernik (chair)
- Denis Greig
- Peter Hatton
- Chris Nicklin
- David Bradley
- Andrew Boothroyd
- Colin Norris

meeting twice a year, in addition to the above, the directors, the chair of the PRP and the beamline team are in attendance.

➡ The Peer Review Panel

The current membership of the panel is as follows:
- Sean Langridge (chair)
- Paul Strange
- Carsten Detlefs
- Steve Collins
- Geetha Balakrishnan
- Karen Edler

In addition either Tom Hase or Chris Lucas attends their meetings.

➡ Housekeeping!!

At the end of your experiment samples should be removed, tools, etc returned to racks and unwanted materials disposed of in appropriately. When travel arrangements are made, therefore, please allow additional time to effect a tidy-up.

➡ PUBLISH PLEASE!!… and keep us informed

Although the list of XMaS papers is growing we still need more of those publications to appear. We ask you to provide Sandra Beaufoy not only with the reference but also a preprint/reprint for our growing collection. Note that the abstract of a publication can also serve as the experimental report!

➡ IMPORTANT!

When beamline staff have made a significant contribution to your scientific investigation you may naturally want to include them as authors. Otherwise we ask that you add an acknowledgement, of the form: "This work was performed on the EPSRC-funded XMaS beamline at the ESRF, directed by M.J. Cooper, C.A. Lucas and T.P.A Hase. We are grateful to S.D. Brown, O. Bikondoa, D. Wermeille, L. Bouchenoire and P. Thompson for their invaluable assistance and to S. Beaufoy and J. Kervin for additional support."

Guidelines
for beam-time applications

➠ Beamline Operation

The XMaS beamline at the ESRF, which came into operation in April 1998, has some 133 days of beam time available each year for UK user experiments, after deducting time allocated for ESRF users, machine dedicated runs and maintenance days. During the year, two long shut-downs of the ESRF are planned: 4 weeks in winter and 4 weeks in summer. At the ESRF, beam is available for user experiments 24 hours a day.

➠ Applications for Beam Time

Two proposal review rounds are held each year, with deadlines for submission of applications, normally, the end of March and September for the scheduling periods August to end of February, and March to July, respectively. Applications for Beam Time are to be submitted electronically (the paper versions are not acceptable) following the successful model used by the ESRF and ourselves. Please consult the instructions given in the ESRF web page:

www.esrf.eu

Follow the links: **"User Portal"** under **"Quick Links"**
Enter your surname and password
and select: **"Proposals/Experiments"**

Follow the instructions carefully – you must choose "CRG Proposal" and "XMAS-BM28" at the appropriate stage in the process. A detailed description of the process is always included in the reminder that is emailed to our users shortly before the deadline – for any problems contact L. Bouchenoire, as above.

Technical specifications of the beamline and instrumentation available are described in the XMaS web page.
When preparing your application, please consider the following:

■ All sections of the form must be filled in. Particular attention should be given to the safety aspects, and the name and characteristics of the substance completed carefully. Experimental conditions requiring special safety precautions such as the use of lasers, high pressure cells, dangerous substances, toxic substances and radioactive materials, must be clearly stated in the proposal. Moreover, any ancillary equipment supplied by the user must conform with the appropriate French regulations. Further information may be obtained from the ESRF Experimental Safety Officer, tel: +33 (0)4 76 88 23 69; fax: +33 (0)4 76 88 24 18.

■ Please indicate your date preferences, including any dates that you would be unable to attend if invited for an experiment. This will help us to produce a schedule that is satisfactory for all.

■ An experimental report on previous measurements must be submitted. New applications will not be considered unless a report on previous work is submitted. These also should be submitted electronically, following the ESRF model. The procedure for the submission follows that for the submission of proposals – again, follow the instructions in the ESRF's web pages carefully. **Reports must be submitted within 6 months of the experiment**.

■ The XMaS beamline is available for one third of its operational time to the ESRF's user community. Applications for beamtime within that quota should be made in the ESRF's proposal round - **Note: their deadlines are earlier than for XMaS! - 1st March and 1st September.** Applications for the same experiment may be made both to XMaS directly and to the ESRF. Obviously, proposals successfully awarded beamtime by the ESRF will not then be given beamtime additionally in the XMaS allocation.

➠ Assessment of Applications

The Peer Review Panel for the UK-CRG considers the proposals, grades them according to scientific excellence, adjusts the requested beam time if required, and recommends proposals to be allocated beam time on the beamline.
Proposals which are allocated beam time must in addition meet ESRF safety and XMaS technical feasibility requirements.
Following each meeting of the Peer Review Panel, proposers will be informed of the decisions taken and some feedback provided.

XMaS the UK-CRG
is an EPSRC sponsored project

XMaS, ESRF, 6 rue Jules Horowitz BP 220, 38043 Grenoble Cedex 9, France
Tel: +33 (0)4 76 88 25 80; Fax: +33 (0)4 76 88 24 55
web page : www.esrf.eu/UsersAndScience/Experiments/CRG/BM28/ – email: boucheno@esrf.fr

Editor: L. Bouchenoire – Layout: ICCS – Print: Warwickprinting – Janvier 2012

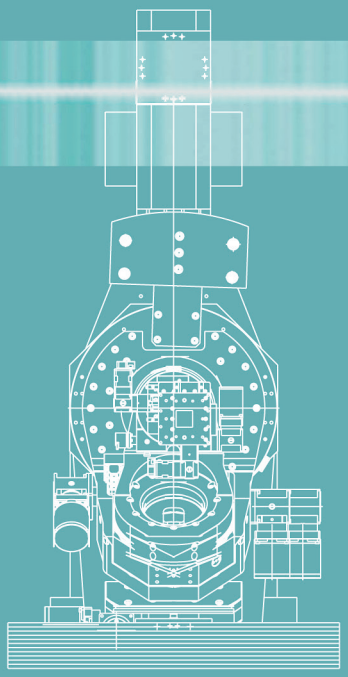

New: Modular Beam Conditioning Unit

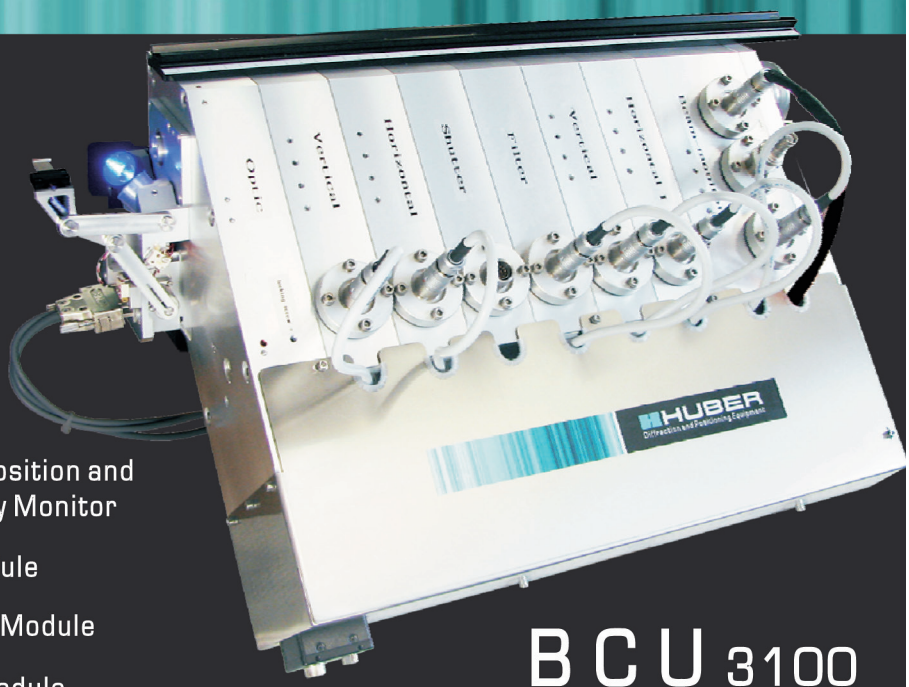

- Beam Position and Intensity Monitor
- Slit Module
- Shutter Module
- Filter Module
- Protein Crystallography Unit

BCU 3100

We make the Best of your Beam

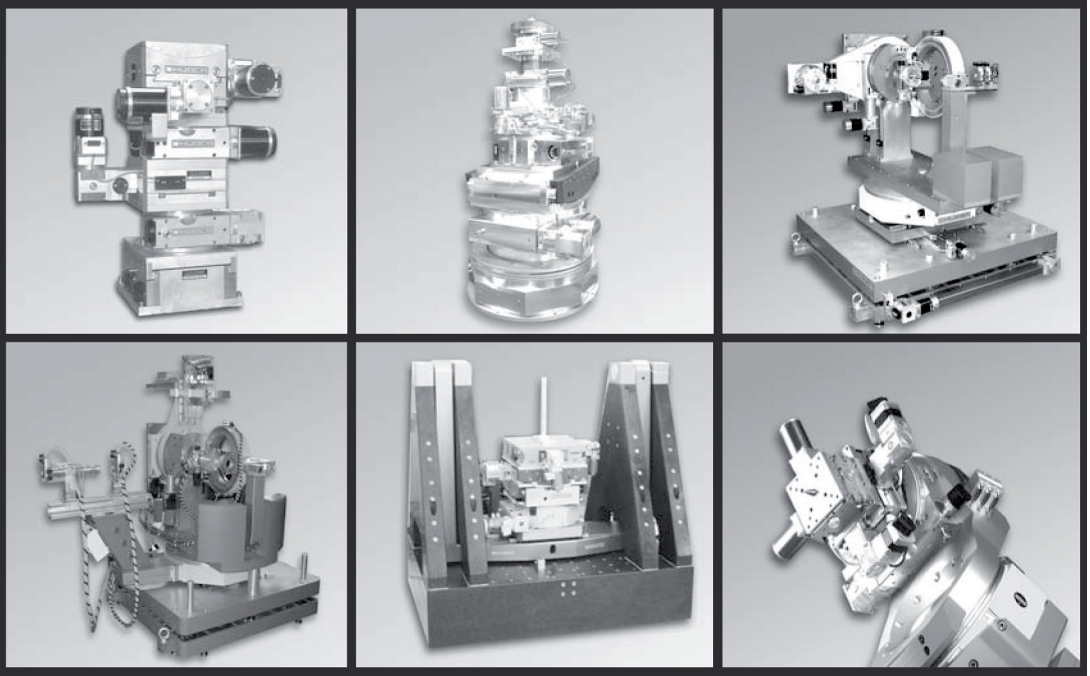

X-Ray Diffractometers and Cameras

Multiaxis Goniometers
for X-Ray-, Synchrotron- and Neutron Facilities

Monochromators

Positioning Devices
for Various Environments

Custom Built Instruments

Electronics

Accessories

HUBER Diffraktionstechnik GmbH & Co. KG
Sommerstrasse 4
D-83253 Rimsting, Germany

www.xhuber.com
info@xhuber.com

HUBER
Diffraction and Positioning Equipment